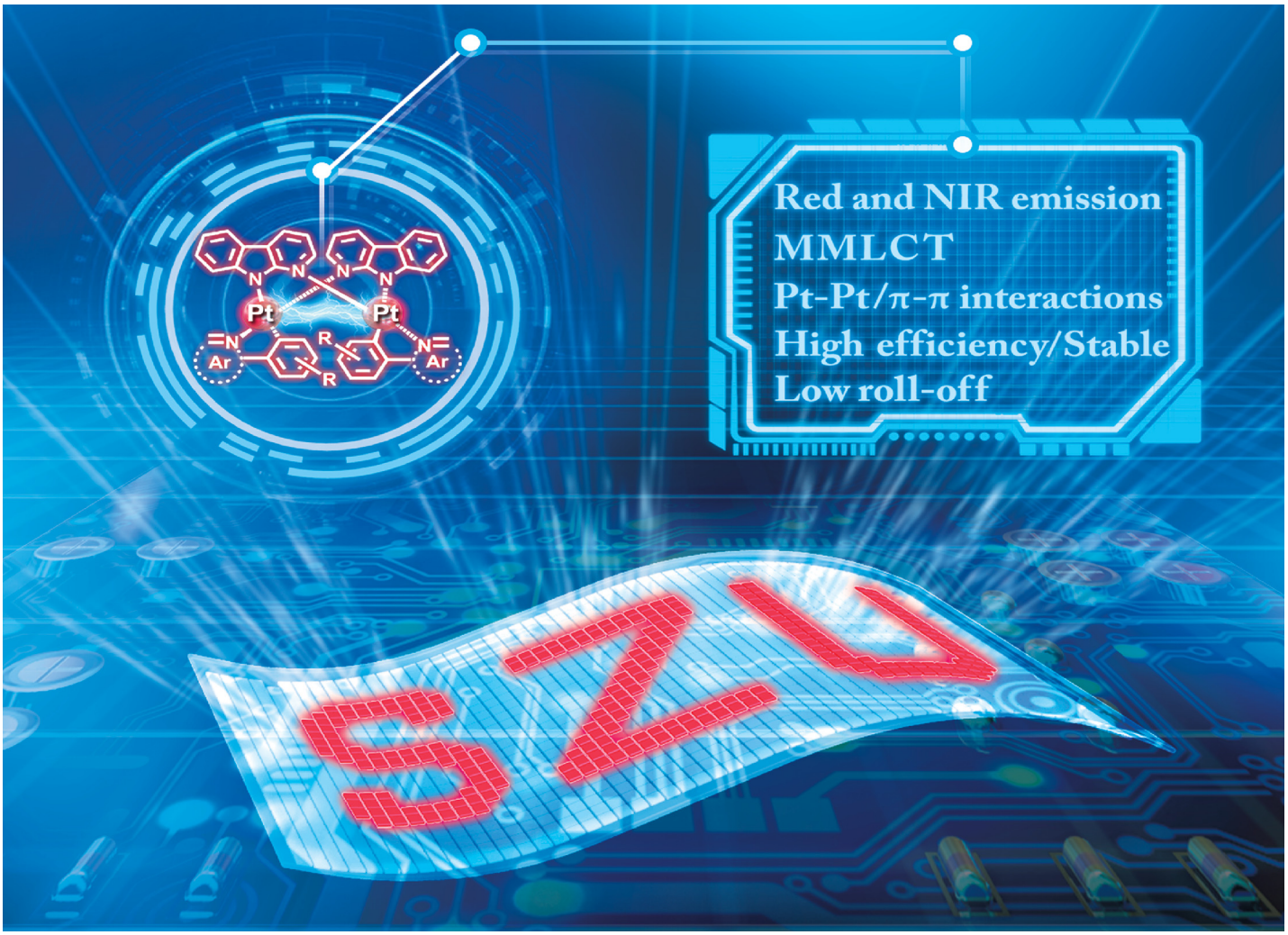

Showcasing research from Professor Kai Li's laboratory, College of Materials Science and Engineering, Shenzhen University, Shenzhen, P. R. China.

High-efficiency and stable red to near-infrared organic light-emitting diodes using dinuclear platinum(II) complexes

High-performance red and NIR organic light-emitting diodes have been achieved using robust diplatinum(II) complexes. The presence of intramolecular Pt–Pt and π–π interactions boosts the radiative decay of the triplet excited states and in the meantime suppresses the nonradiative decay.

As featured in:

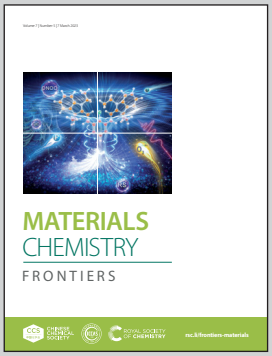

See Youming Zhang, Kai Li *et al.*, *Mater. Chem. Front.*, 2023, **7**, 873.

CCS 中国化学会 CHINESE CHEMICAL SOCIETY
ICCAS
ROYAL SOCIETY OF CHEMISTRY
rsc.li/frontiers-materials

MATERIALS CHEMISTRY
FRONTIERS

CHINESE CHEMICAL SOCIETY

ROYAL SOCIETY OF CHEMISTRY

RESEARCH ARTICLE

View Article Online
View Journal | View Issue

Cite this: *Mater. Chem. Front.*, 2023, 7, 873

High-efficiency and stable red to near-infrared organic light-emitting diodes using dinuclear platinum(II) complexes†

Lian Wang,‡ Zhenhua Wen,‡ Yulin Xu, Youming Zhang,* Jingsheng Miao, Zhanxiang Chen and Kai Li *

Received 12th November 2022,
Accepted 30th January 2023

DOI: 10.1039/d2qm01163h

rsc.li/frontiers-materials

Increasing the radiative decay rates of triplet excited states to overcome the energy-gap law is important for the development of high-efficiency and short-lived phosphorescent metal complexes in the red to near-infrared (NIR) region. Herein, a series of robust dinuclear Pt(II) complexes featuring strong intramolecular noncovalent Pt–Pt and π–π interactions has been developed by using *N*-deprotonated α-carboline as the bridging ligands. Combined crystallography, electrochemical and computational studies reveal their rigid structures and triplet metal–metal-to-ligand charge transfer (^{3}MMLCT) excited states. The new complexes exhibit efficient red to NIR phosphorescence with excited lifetimes shorter than 2 μs. Organic light-emitting diodes (OLEDs) doped with these complexes show high maximum external quantum efficiencies (EQEs) up to 26.4% (λ_{max} = 615 nm) and 10.8% for red and NIR (λ_{max} = 740 nm) devices, respectively, which are among the best devices doped with discrete Pt(II) complexes. Both the red and NIR devices also show small efficiency roll-offs at high brightness. Appealing operational lifetimes have also been revealed which promise their practicality.

1. Introduction

Red and near-infrared (NIR) organic light-emitting diodes (OLEDs) have attracted much attentions because of their potential applications in various fields.[1] However, according to the energy-gap law, the non-radiative decay rate of a molecular excited state increases exponentially as the excited state energy decreases, which hinders the development of high-efficiency red and NIR emitters.[2] In the context of red phosphorescent molecular emitters, iridium(III) complexes have been shown to be superior to afford high photo- and electroluminescence efficiencies because of their facilely accessible triplet metal-to-ligand charge transfer (^{3}MLCT) excited states.[3] This is due to the fact that the strong spin-orbit coupling (SOC) effect arising from the large metal parentage in the ^{3}MLCT excited state can significantly promote the radiative decay (k_r) process.[4] Alternatively, moderate-to-high red phosphorescence efficiencies from triplet intraligand (^{3}IL) excited states of other transition metals have only been scarcely achieved by using rigid ligands for suppression of the excited state geometry distortions.[5] However, NIR phosphorescence efficiencies based on these two design tactics have been still lower than those of the green and blue emitting complexes. Indeed, the external quantum efficiencies (EQEs) of NIR devices can hardly exceed 10%.[6] Therefore, it is still of great importance to explore new approach for developing efficient red phosphorescent metal complexes without using iridium and for overcoming the efficiency limit of NIR phosphorescence.

To this end, it is obvious that tuning of the triplet excited states to have fast radiative decay rates is essential. In the meantime, a fast radiative decay would lead to short emission lifetimes which are critical to high-performance OLEDs with high maximum brightness, small efficiency roll-off, and long device lifespan. In this context, aggregation of Pt(II) complexes driven by intermolecular Pt–Pt and π–π interactions have been comprehensively explored which are pioneered by Chi and co-workers.[7] It has been well established that the metallophilic interactions can generate triplet metal–metal-to-ligand charge transfer (^{3}MMLCT) excited states which are typically characterized by high radiative decay rates.[8] Further, in comparison with their mononuclear analogues, the emission energies of ^{3}MMLCT excited states are significantly smaller. Both these features suggest the ^{3}MMLCT excited states of Pt(II) complexes to be a promising solution to red and NIR phosphorescent emitters. Remarkably, recent efforts to suppress the vibronic-coupling between the excited state and the ground state through exciton delocalization and/or ligands deuteration have led

Shenzhen Key Laboratory of New Information Display and Storage Materials, College of Materials Science and Engineering, Shenzhen University, Shenzhen 518055, P. R. China. E-mail: zhangym@szu.edu.cn, kaili@szu.edu.cn

† Electronic supplementary information (ESI) available. CCDC 2209083, 2209084, 2209085 and 2209086. For ESI and crystallographic data in CIF or other electronic format see DOI: https://doi.org/10.1039/d2qm01163h

‡ These authors contributed equally to this work.

to record-high NIR phosphorescence efficiencies.[7f,g] Regarding the interesting properties of ^{3}MMLCT excited states, dinuclear platinum complexes with close intramolecular Pt–Pt contacts have also received much attentions over decades.[8a,b,9] For example, butterfly-shaped dinuclear Pt(II) complexes with pyrazolate as the bridging ligands were studied in detail to decipher the excited state structural changes in terms of Pt–Pt shortening.[10] These type of complexes have been exploited as sensory materials on the basis of the fact that the Pt–Pt interactions are sensitive to the physicochemical properties of local media.[11] Thiazol-2-thiolate, hydroxypyridine, and ditopic bis-μ_2-formamidinate were also used as the bridging ligands to construct half-lantern Pt(II) complexes exhibiting moderate-to-intense phosphorescence.[12] However, their potentials as OLED emitters have been overlooked for a long time and only few studies have emerged recently.[13]

We conceived that the use of highly rigid bridging ligand to confine Pt–Pt alignment would be feasible for the development of robust and efficient red and NIR Pt(II) emitters for OLEDs. To testify this, we synthesized a class of dinuclear Pt(II) complexes bridged by *N*-deprotonated α-carboline. The emitters delivered efficient red and NIR electroluminescence and appealing device operation stability.[14] These performances provided impetus to us to perform comprehensive studies on this type of complexes and to further develop red and NIR emitters by molecular structural modifications. In this work, four new Pt(II) complexes (**Pt-1**, **Pt-2**, **Pt-3** and **Pt-4**) were synthesized by using 2-(4-fluorophenyl)pyridine (Fppy), 2-(5-methylthiophen-2-yl)pyridine (Methpy), 2-(2,4-difluorophenyl)pyrimidine (2Fppyr) and 1-phenylisoquinoline (piq) as the C^N ligands (Scheme 1). Electrochemical studies revealed good redox reversibility for all the complexes which should secure a good electrochemical stability in operating devices. Theoretical studies showed small excited state structural distortions for these complexes owing to the rigid scaffold of the bridge. Together with their ^{3}MMLCT excited states, the new complexes demonstrated high-performance red and NIR OLEDs with maximum external quantum efficiencies (EQEs) up to 26.5% (λ_{max} = 615 nm) and 10.8% (λ_{max} = 740 nm), respectively. More importantly, the devices show small roll-offs at high brightness and appealing operational lifetimes which are among the best red and NIR device performances using discrete Pt(II) complexes.

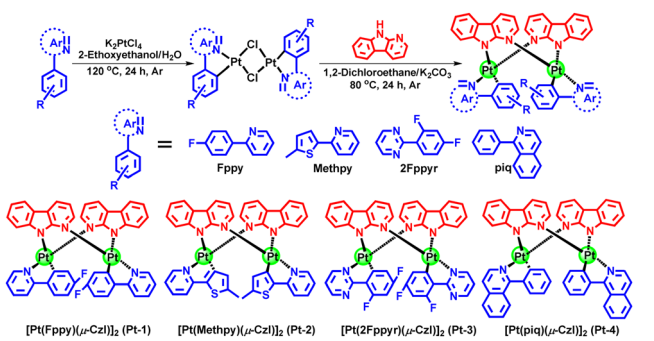

Scheme 1 Synthesis and structures of dinuclear Pt(II) complexes **Pt-1**, **Pt-2**, **Pt-3** and **Pt-4**.

2. Results and discussion

2.1. Synthesis and characterization

Complexes **Pt-1**–**Pt-4** were synthesized according to the method reported elsewhere (Scheme 1).[14] The complexes were purified through column chromatography and sublimation (temperature ~350 °C; pressure $<10^{-4}$ Pa). Their molecular structures were characterized by ^{1}H NMR spectroscopy, high resolution mass spectrometry (HRMS), elemental analysis (EA) and single-crystal X-ray diffraction studies. Thermogravimetric analysis (TGA) showed decomposition temperatures (T_d at 5% weight loss) of 460, 436, 362 and 374 °C for **Pt-1**, **Pt-2**, **Pt-3** and **Pt-4** in N_2 atmosphere, respectively (Fig. S1, ESI† and Table 1). The present diplatinum(II) complexes have excellent thermal stability for OLED fabrications *via* vacuum deposition. Comparing with Pt(II) complexes supported by tetradentate ligands which have been highly sought after because of the chelating effect of ligands,[15] the leveraging of intramolecular noncovalent interactions suggests a promising way to robust emitters.[16]

To acquire the structural parameters which are key to ^{3}MMLCT emission properties, single crystals of all the four complexes were grown for X-ray diffraction studies. Full crystallographic information in CIF format has been deposited at the Cambridge Crystallographic Data Center (CCDC†) under deposition numbers 2209083, 2209084, 2209085 and 2209086 for **Pt-1**, **Pt-2**, **Pt-3** and **Pt-4**, respectively. The crystal data and structure refinements for all the complexes are summarized in Table S1 (ESI†). As shown in Fig. 1, the two C^N ligands and the two α-carboline bridges in all complexes are arranged with opposite directions. The distances between Pt atoms were determined to be *ca.* 2.95–2.96 Å, which are within the typical values for 4-bond bridged dinuclear Pt(II) complexes.[12a,c,e,13b] Although there is a small angle between the C^N ligand planes for all complexes, short π–π contacts (*ca.* 3.5 Å, Fig. 1) are still observed between them. These structural features manifest the significant noncovalent Pt–Pt/π–π interactions, which should favour the generation of ^{3}MMLCT excited states. In the crystal packing diagrams, different stacking patterns were noted for these complexes (Fig. S2 and S3, ESI†). Of note is the one-dimensional stacking of **Pt-3** molecules through short intermolecular π–π and H-bonding interactions due to the presence of fluorine atoms.

2.2. Electrochemical properties

The electrochemical properties of all the four complexes were studied by cyclic voltammetry in dichloromethane (DCM).

Table 1 Electrochemical and thermal parameters for complexes

	E_{ox}[a] (V)	E_{red}[a] (V)	E_{HOMO}[b] (eV)	E_{LUMO}[c] (eV)	E_{opt}[d] (eV)	T_d[e] (°C)
Pt-1	0.66	—	−4.94	−2.66	2.28	460
Pt-2	0.60	—	−4.88	−2.68	2.20	436
Pt-3	0.63	−1.55	−4.91	−2.71	2.20	362
Pt-4	0.56	−1.60	−4.84	−2.92	1.92	374

[a] Measured by cyclic voltammetry. [b] $E_{HOMO} = -[(E_{ox}-0.52) + 4.8]$ eV, where 0.52 V denotes the $E(Cp_2Fe^{+/0})$ *vs.* Ag/AgCl and −4.8 eV is the energy level of ferrocene relative to the vacuum. [c] $E_{LUMO} = E_{opt} + E_{HOMO}$. [d] E_{opt} = 1240/$\lambda_{abs,onset}$, where $\lambda_{abs,onset}$ is the absorption onset. [e] The temperature at a weight loss of 5% in an N_2 atmosphere.

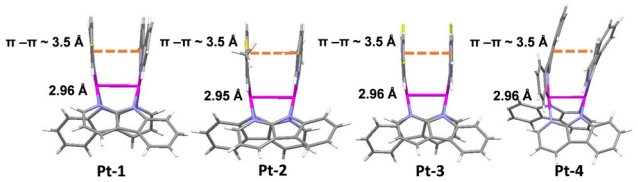

Fig. 1 Perspective views of the X-ray crystal structures of **Pt-1**, **Pt-2**, **Pt-3** and **Pt-4**.

The cyclic voltammograms are shown in Fig. S4 (ESI†) and the pertinent data are collected in Table 1. The reversible oxidation potentials for all complexes were observed at 0.66, 0.60, 0.63 and 0.56 V *versus* Ag/AgCl for **Pt-1**, **Pt-2**, **Pt-3** and **Pt-4**, respectively. With reference to the previous report, the oxidations are assigned to take place on the carboline ligands and metal atoms.[14] The energy levels of HOMO (E_{HOMO}) are estimated to be −4.94, −4.88, −4.91 and −4.84 eV for **Pt-1**, **Pt-2**, **Pt-3** and **Pt-4** by using the $Cp_2Fe^{+/0}$ as the internal reference. It has been pointed out that the oxidations of dinuclear Pt(II) complexes have improved reversibility, implying better electrochemical stability in operating devices.[12c,12e,17] Regarding the reductions, waves were only found for **Pt-3** and **Pt-4** which located at −1.55 and −1.60 V *versus* Ag/AgCl, respectively. The cathodic shift for **Pt-4** in comparison with **Pt-3** supports the assignment of these waves to the reductions of cyclometalating C^N ligands. For illustrating the tuning of excited state energy by varying the C^N ligands, the energy levels of the lowest unoccupied molecular orbital (LUMO) (E_{LUMO}) for all complexes are estimated based on their HOMO levels and optical bandgaps. The gradual decrease in LUMO from −2.66 eV for **Pt-1** to −2.92 eV for **Pt-4** is consistent with their absorption and emission energies.

2.3. Photophysical properties

As depicted in Fig. 2A, the diluted solutions of Pt(II) complexes in DCM exhibit characteristic low-energy ^{1}MMLCT absorptions with absorption maxima at 550–620 nm. Upon photo-excitation, they show red to NIR emissions peaked at 621, 602, 645 and 740 nm at room temperature (Fig. 2 and Table 2). For **Pt-2**, the replacement of phenyl ring by a thiophenyl ring in the C^N ligands results in a slightly different emission spectral profile which has a shoulder at 640 nm. In 10 wt% doped polymethyl methacrylate (PMMA), all complexes exhibit intense photoluminescence with maxima of 596–692 nm (Fig. 2B). The emission quantum yields (Φ) were determined to be 67%, 49%, 45% and 29% for **Pt-1**, **Pt-2**, **Pt-3** and **Pt-4**, respectively. As expected, all the complexes have short emission lifetimes in the range of 0.8–1.9 μs (Fig. 2C and Table 2). The estimated k_r values of 2.6×10^5–3.9×10^5 are consistent with their ^{3}MMLCT nature (Table 2).

Although the stacking of Pt(II) complexes is highly desired for fabrication of non-doped devices, it is important to reduce the concentration-dependence of the emission properties of dinuclear Pt(II) complexes for doped device fabrications. Therefore, the PL properties of **Pt-1**–**Pt-4** in PMMA at various dopant concentrations (10–60 wt%) and in neat films were examined. As depicted in Fig. 2B, increasing the doping concentration

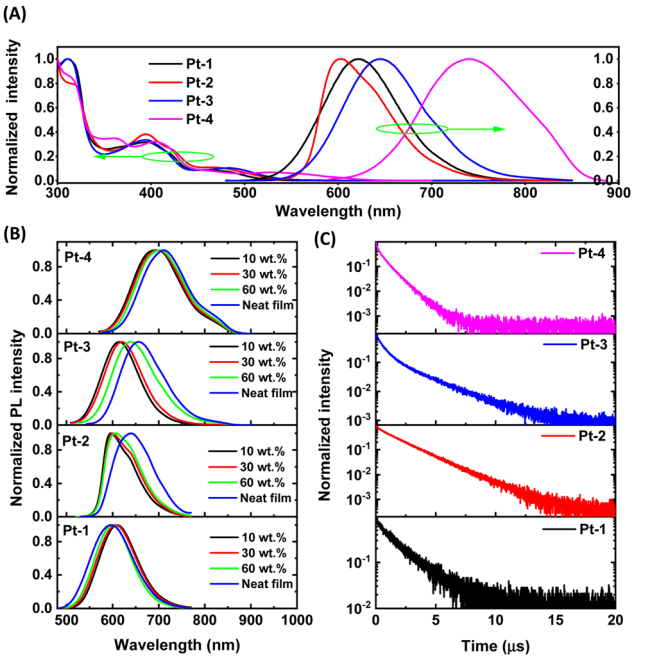

Fig. 2 (A) UV/Vis absorption and photoluminescence (PL) spectra of **Pt-1**–**Pt-4** in DCM (10^{-5} M). (B) PL spectra of **Pt-1**–**Pt-4** in PMMA at various concentrations (10 wt%, 30 wt%, and 60 wt%) and in neat film. (C) PL decay characteristics of **Pt-1**–**Pt-4** in PMMA (10 wt%) in Ar.

Table 2 Photophysical data for the Pt(II) complexes

	λ_{abs}[a] (nm)	λ_{em}[b] (nm)	τ[c] (μs)	Φ[d] (%)	k_r[e] (10^5 s^{-1})	k_{nr}[e] (10^5 s^{-1})
Pt-1	462	621/597	1.7	67	3.9	1.9
Pt-2	465	602/596	1.9	59	3.1	2.2
Pt-3	485	645/614	1.7	45	2.6	3.2
Pt-4	525	740/692	0.8	29	3.6	8.8

[a] The ^{1}MMLCT absorption maxima in solution. [b] In deaerated dichloromethane (10^5 M, left) and 10 wt% doped PMMA film (right). [c] For the 10 wt% doped PMMA film in Ar. [d] Absolute photoluminescence quantum yield determined using an integrating sphere for the 10 wt% doped PMMA film in Ar. [e] Calculated using $k_r = \Phi/\tau$ and $k_{nr} = (1-\Phi)/\tau$.

from 10 wt% to 30 wt% did not lead to notable change in emission spectra for each complex, after which redshifts were observed for **Pt-3** and **Pt-4**. Notably, a large redshift (43 nm) for **Pt-2** was only observed in its neat film. Interestingly, a slight hypsochromic shift (*ca.*10 nm and 0.01 eV) occured for **Pt-1** in its neat film, presumably due to a different stacking effect. In brief, the moderate-to-high emission efficiencies and short lifetimes make this type of complexes promising emitters for the fabrication of doped OLEDs.

2.4. Theoretical calculations

To gain insight into the structural and electronic properties of the present diplatinum(II) complexes, quantum calculations were performed using the Gaussian 09 program at the B3LYP/6-31G(d) level. First, to unveil the rigidity of the complex skeletons which is crucial to suppress excited state non-radiative decay, we calculated the root-mean-square displacements (RMSD) between the optimized T_1 and S_0 geometries. The RMSD values are 0.387,

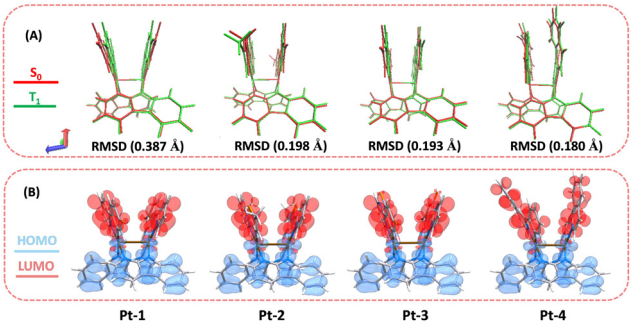

Fig. 3 (A) Comparison of the optimized S_0 (red) and T_1 (green) structures for **Pt-1**–**Pt-4**. (B) HOMO (blue)–LUMO (red) for **Pt-1**–**Pt-4** in S_0 state.

0.198, 0.193 and 0.180 Å for **Pt-1**, **Pt-2**, **Pt-3** and **Pt-4**, respectively (Fig. 3A), revealing relatively small excited state structural changes. As shown in Fig. 3B, the HOMOs of all complexes in S_0 state are mainly distributed over the carboline skeletons and platinum atoms. The LUMOs are dominated by the C^N ligands. Therefore, excitation of the complexes correspond to a mixed MMLCT and ligand-to-ligand charge transfer (LLCT) transition. Further, by taking **Pt-1** and **Pt-2** as examples, the spin-orbit coupling (SOC) interactions (ξ) between S_1/T_1 and S_0 states were calculated to understand the intersystem crossing (ISC) processes (Fig. S5, ESI†). The ξ (S_0, T_1) and ξ (S_1, T_1) are 638 and 221 cm^{-1} for **Pt-1** and 153 and 457 cm^{-1} for **Pt-2**. Of note, these values are comparable to that of the prototypical red-emitting Ir(III) complex with ^{3}MLCT excited states and much higher than that of the well-known red-emitting tetradentate Pt(II) complex which are calculated using the same method (Fig. S5, ESI†).[3d,5b] In all, the restricted excited state geometry change and enhanced SOC effect stemming from the dinuclear rigid structural scaffold make this kind of complexes ideal red and NIR emitters for OLEDs.

2.5. Electroluminescence performance

The electroluminescence (EL) properties of **Pt-1**–**Pt-4** were studied using vacuum deposited device with a structure of ITO/HAT-CN (5 nm)/TAPC (30 nm)/TCTA (15 nm)/DMIC-CZ + DMIC-TRZ: emitter (50 nm)/ANT-BIZ (30 nm)/Liq (2 nm)/Al (100 nm). The chemical structures of 1,4,5,8,9,11-hexaazatriphenylenehexacarbonitrile (HATCN), 1,1-bis[(di-4-tolylamino)phenyl]cyclohexane (TAPC), tris(4-carbazolyl-9-ylphenyl)amine (TCTA), 1-[4-(10-[1,1′-biphenyl]-4-yl-9-anthracenyl)phenyl]-2-ethyl-1*H*-benzimidazole(ANT-BIZ), 5,7-dihydro-7,7-dimethyl-5-phenyl-3-(9-phenyl-9*H*-carbazol-3-yl)-indeno -[2,1-*b*]carbazole (DMIC-CZ) and 1,3-dihydro-1,1-dimethyl-3-(3-(4,6-diphenyl-1,3,5-triazin-2-yl)phenyl)indeno-[2,1-*b*]carbazole (DMIC-TRZ) are shown in Fig. S6 (ESI†). The HATCN, TAPC, TCTA, and ANTBIZ are employed as hole-injection, hole-transporting, electron-blocking, and electron-transporting layers, respectively. A mixture consisting of DMIC-CZ and DMIC-TRZ was used as the co-host because of their low charge injection barrier between the charge-transport layers and the emitting layer, reduced quenching of the triplet–polaron and triplet–triplet annihilation, and both efficient Dexter and Förster energy transfer from host to guest.[18] The device performances at various dopant concentrations are presented in Fig. S7–S10 and

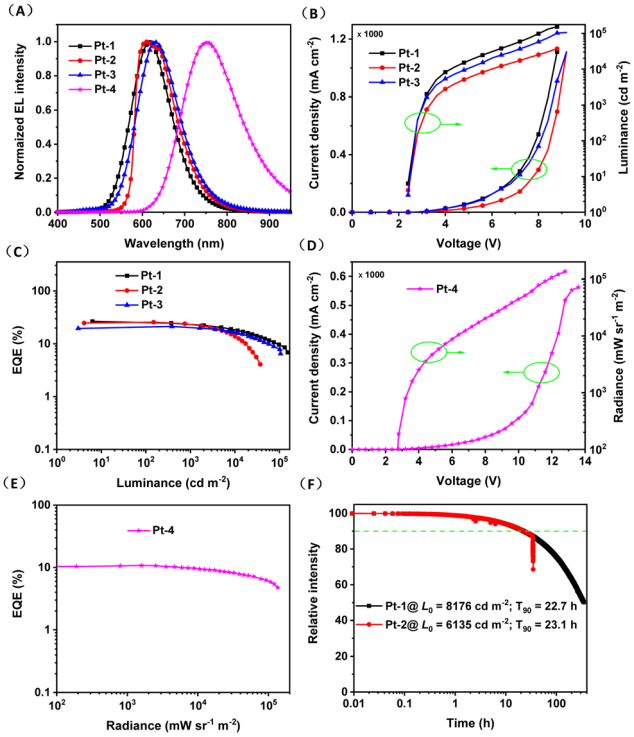

Fig. 4 (A) Normalized EL spectra of the selected red and NIR devices doped with **Pt-1** (6 wt%), **Pt-2** (9 wt%), **Pt-3** (6 wt%) and **Pt-4** (3 wt%). (B) *J*–*V*–*L* characteristics and (C) EQE *versus* the luminance of the red OLEDs doped with **Pt-1** (6 wt%), **Pt-2** (9 wt%) and **Pt-3** (6 wt%). (D) *J*–*V*–*R* characteristics and (E) EQE *versus* the radiance of the NIR OLEDs doped with **Pt-4** (3 wt%). (F) Normalized EL intensity of the device *versus* operating time.

Tables S2–S5 (ESI†). The optimized device data for **Pt-1** (6 wt%), **Pt-2** (9 wt%), **Pt-3** (6 wt%) and **Pt-4** (3 wt%) are also summarized in Fig. 4 and Table 3. The maximum EQEs for red OLEDs based on **Pt-1**, **Pt-2** and **Pt-3** are 26.4% (λ_{EL} = 615 nm), 25.7% (λ_{EL} = 610 nm) and 21.3% (λ_{EL} = 630 nm), respectively. These values are on par with the highest EQEs for red OLEDs based on discrete complexes without using iridium element. Of note, the narrower and slightly vibronically resolved spectrum was observed for **Pt-2**, which should be responsible for its larger CIE_x value comparing with **Pt-1** and **Pt-3**. For **Pt-4** based device, the maximum EQE is 10.8% (λ_{EL} = 740 nm) which is among the record-high doped NIR device efficiencies at wavelengths beyond 740 nm based on phosphorescent and fluorescent emitters.[6d,19] Moreover, the EQEs for **Pt-1**, **Pt-2** and **Pt-3** based devices at 10 000 cd m^{-2} are

Table 3 Key device data for selected red and NIR OLEDs

	λ_{EL} [a] (nm)	L_{max} [b] (cd m^{-2}) or R_{max} [c] (mW sr^{-1} m^{-2})	EQE_{max} (%)	CIE (x, y)
Pt-1	615	153 065[b]	26.4/20.0[d]	(0.59, 0.41)
Pt-2	610	37 142[b]	25.7/18.2[d]	(0.64, 0.36)
Pt-3	630	106 231[b]	21.3/18.5[d]	(0.62, 0.38)
Pt-4	740	1 361 325[c]	10.8/9.5[e]	(0.66, 0.36)

[a] Wavelength of the EL maximum. [b] Maximum luminance. [c] Maximum radiance. [d] Maximum/@10 000 cd m^{-2}. [e] Maximum/@10 000 mW sr^{-1} m^{-2}.

maintained at 20.0%, 18.2% and 18.5%. The **Pt-4** based devices show EQEs of 9.5% and 6.1% at 10/100 W sr^{-1} m^{-2}, respectively. Their short phosphorescence lifetimes are surmised to be crucial to the little device efficiency roll-offs at high brightness because the triplet excited state saturation can be avoided.

The operational stability of devices based on **Pt-1** and **Pt-2** was tested in the same abovementioned device structure. For the test, the devices were driven at a constant current of 3 mA, corresponding to an initial luminance (L_0) of 8176 and 6135 cd m^{-2} for **Pt-1** and **Pt-2**. As depicted in Fig. 4F, the T_{90} (the time required for the luminance to drop to 90% of initial value) were recorded to be 22.7 and 23.1 h for **Pt-1** and **Pt-2**, respectively. By roughly assuming a moderate acceleration factor of 1.7 according to the stretched exponential decay equation of $T(L_1) = T(L_0)(L_0/L_1)^n$, the T_{90} at 1000/100 cd m^{-2} are estimated to be 808/39 954 h for **Pt-1** and 505/25 300 h for **Pt-2**, which are superior than the device performances of tetradentate Pt(II) complexes.[5b,c] On the other hand, a half lifetime (T_{50}) of 350 h was recorded for **Pt-1** based device, translating to half-decay lifetimes of 12 456 and 624 291 h with initial luminance at 1000 and 100 cd m^{-2}, respectively.

3. Conclusions

In summary, four new diplatinum(II) complexes using *N*-deprotonated α-carboline as the bridging ligands have been developed. The aromatic bridges rigidify the double-decker molecular configuration to have close intramolecular Pt–Pt and π–π contacts. The geometrical and electronic structures of the complexes result in highly emissive ^{3}MMLCT states in the red and NIR region with emission lifetimes shorter than 2 μs. Thermal and electrochemical studies also revealed their good stability. All complexes have been used for fabrications of OLEDs *via* vacuum deposition. The devices showed high efficiencies with maximum EQEs of up to 26.4% and 10.8% for red and NIR phosphorescence, respectively. Furthermore, a half lifetime (T_{50}) of over 0.6 million hours at 100 cd m^{-2} has been estimated for a red OLED. The device performances indicate that this type of molecules can be exploited as phosphorescent emitters for efficient and stable devices.

4. Experimental section

4.1. Materials and reagents

All synthesis experiments involving oxygen-sensitive reagents were performed in argon. 2-(4-fluorophenyl)pyridine (Fppy), 2-(5-methylthiophen-2-yl)pyridine (Methpy), 2-(2,4-difluorophenyl)-pyrimidine (2Fppyr), 1-phenylisoquinoline (piq), α-carboline (Czl) and potassium tetrachloroplatinate(II) (K_2PtCl_4) as well as the solvents were purchased and used as received without further purification.

4.2. General procedure for synthesis of the Pt(II) complexes

A mixture of C^N ligand (1 equiv.), K_2PtCl_4 (1 equiv.) in 2-ethoxyethanol and water (3 : 1, v/v) was heated at 120 °C with stirring in an argon atmosphere for 24 h. After cooling to room temperature, it was poured into water, and the resulting precipitate was filtered and washed with water to obtain the dimer. This dimer was used for the next step without any further purification. A mixture of the dimer intermediate, α-carboline (2.5 equiv.), and K_2CO_3 (3 equiv.) in DCM was stirred at 80 °C for 24 h in an argon atmosphere. Then the solvent was removed under reduced pressure, and the residue was purified through column chromatography using petroleum ether and DCM as the eluent to give the products as orange to crimson powder.

[Pt(Fppy)(μ-Czl)]$_2$ (Pt-1), orange red solid (yield: 37%). ^{1}H NMR (500 MHz, methylene chloride-d_2) δ 8.64 (dd, J = 5.8, 1.4 Hz, 2H), 8.37–8.22 (m, 4H), 8.03 (d, J = 7.7 Hz, 2H), 7.75–7.59 (m, 2H), 7.45 (ddd, J = 8.3, 7.1, 1.3 Hz, 2H), 7.38 (td, J = 7.8, 1.7 Hz, 2H), 7.19–7.11 (m, 4H), 7.07 (dd, J = 8.5, 5.5 Hz, 2H), 6.83 (dd, J = 7.5, 5.8 Hz, 2H), 6.49 (td, J = 8.8, 2.6 Hz, 2H), 6.31 (ddd, J = 7.3, 5.7, 1.4 Hz, 2H), 5.74 (dd, J = 9.7, 2.6 Hz, 2H). HRMS (ESI) m/z calcd for $C_{44}H_{29}F_2N_6Pt_2$ $[M + H]^+$: 1069.1639, found: 1069.1690. Analy. calcd for $C_{44}H_{28}F_2N_6Pt_2$: C, 49.44; H, 2.64; N, 7.86; found: C, 49.68; H, 2.24; N, 7.80.

[Pt(Methpy)(μ-Czl)]$_2$ (Pt-2), red solid (yield: 27%). ^{1}H NMR (500 MHz, methylene chloride-d_2) δ 8.68 (dd, J = 5.8, 1.4 Hz, 2H), 8.29 (dt, J = 8.2, 0.9 Hz, 2H), 8.25 (dd, J = 7.4, 1.4 Hz, 2H), 8.01 (dt, J = 7.7, 1.0 Hz, 2H), 7.44 (ddd, J = 8.3, 7.1, 1.3 Hz, 2H), 7.34 (dd, J = 8.0, 6.4 Hz, 4H), 7.13 (ddd, J = 8.0, 7.2, 1.0 Hz, 2H), 6.82–6.77 (m, 4H), 6.13 (td, J = 6.9, 6.4, 1.4 Hz, 2H), 5.56–5.47 (m, 2H), 2.22 (d, J = 1.1 Hz, 6H). HRMS (ESI) m/z calcd for $C_{42}H_{29}N_6Pt_2S_2$ $[M-H]^+$: 1071.1269, found: 1071.1263. Analy. calcd for $C_{42}H_{30}N_6Pt_2S_2$: C, 47.01; H, 2.82; N, 7.83; found: C, 47.02; H, 2.96; N, 7.77.

[Pt(2Fppyr)(μ-Czl)]$_2$ (Pt-3), red solid (yield: 31%). ^{1}H NMR (400 MHz, methylene chloride-d_2) δ 8.64–8.36 (m, 4H), 8.21 (dd, J = 7.5, 1.4 Hz, 2H), 8.18–8.11 (m, 2H), 7.96 (dt, J = 7.8, 1.0 Hz, 2H), 7.85 (dd, J = 5.8, 2.3 Hz, 2H), 7.41 (ddd, J = 8.3, 7.2, 1.3 Hz, 2H), 7.10 (ddd, J = 8.0, 7.2, 1.0 Hz, 2H), 6.78 (dd, J = 7.5, 5.9 Hz, 2H), 6.37–6.22 (m, 4H), 5.54 (dd, J = 8.5, 2.4 Hz, 2H). HRMS (ESI) m/z calcd for $C_{42}H_{25}F_4N_8Pt_2$ $[M + H]^+$: 1107.1356, found: 1107.1410. Analy. calcd for $C_{42}H_{24}F_4N_8Pt_2$: C, 45.58; H, 2.19; N, 10.12; found: C, 45.64; H, 2.60; N, 9.93.

[Pt(piq)(μ-Czl)]$_2$ (Pt-4), crimson solid (yield: 28%). ^{1}H NMR (500 MHz, methylene chloride-d_2) δ 8.56 (dd, J = 5.7, 1.5 Hz, 2H), 8.24 (d, J = 8.2 Hz, 2H), 8.19 (dd, J = 7.5, 1.5 Hz, 2H), 7.96 (dt, J = 7.7, 1.0 Hz, 2H), 7.88 (d, J = 8.7 Hz, 2H), 7.70 (d, J = 6.4 Hz, 2H), 7.53 (ddd, J = 8.0, 6.7, 1.1 Hz, 2H), 7.49–7.44 (m, 2H), 7.36 (ddd, J = 8.2, 7.0, 1.2 Hz, 2H), 7.32 (ddd, J = 8.5, 6.8, 1.5 Hz, 2H), 7.06 (ddd, J = 8.0, 7.1, 1.0 Hz, 2H), 7.00 (dd, J = 7.2, 2.2 Hz, 2H), 6.72 (dd, J = 7.5, 5.7 Hz, 2H), 6.47 (td, J = 5.8, 2.8 Hz, 6H), 6.16–6.05 (m, 2H). HRMS (ESI) m/z calcd for $C_{52}H_{35}N_6Pt_2$ $[M + H]^+$: 1133.2140, found: 1133.2171. Analy. calcd for $C_{52}H_{34}N_6Pt_2$: C, 55.12; H, 3.02; N, 7.42 found: C, 55.21; H, 2.62; N, 7.24.

Author contributions

K. L. and Y. Z. conceived the project. L. W. and Z. W. performed the materials synthesis, structural characterizations, and photophysical

measurements. Y. X. and J. M. fabricated and tested the OLEDs. Y. Z. and Z. C. carried out the theoretical calculations. Y. Z. and K. L. wrote the paper. All authors discussed the results and commented on the manuscript.

Conflicts of interest

The authors declare no conflict interests.

Acknowledgements

This research was financially supported by the National Natural Science Foundation of China (51903157 and 52130308) and the Shenzhen Science and Technology Program (KQTD20170330110107046 and ZDSYS20210623091813040). We thank the Instrumental Analysis Center of Shenzhen University for analytical support.

Notes and references

1 (*a*) H. Xiang, J. Cheng, X. Ma, X. Zhou and J. J. Chruma, Near-infrared phosphorescence: materials and applications, *Chem. Soc. Rev.*, 2013, **42**, 6128–6185; (*b*) Y. Zhang, Y. Wang, J. Song, J. Qu, B. Li, W. Zhu and W.-Y. Wong, Near-infrared emitting materials via harvesting triplet excitons: molecular design, properties, and application in organic light emitting diodes, *Adv. Opt. Mater.*, 2018, **6**, 1800466; (*c*) S. Yoon and T. S. Teets, Red to near-infrared phosphorescent Ir(III) complexes with electron-rich chelating ligands, *Chem. Commun.*, 2021, **57**, 1975–1988; (*d*) M. Vasilopoulou, A. Fakharuddin, F. P. García de Arquer, D. G. Georgiadou, H. Kim, A. R. B. Mohd Yusoff, F. Gao, M. K. Nazeeruddin, H. J. Bolink and E. H. Sargent, Advances in solution-processed near-infrared light-emitting diodes, *Nat. Photonics*, 2021, **15**, 656–669; (*e*) Y. Zhang and J. Qiao, Near-infrared emitting iridium complexes: Molecular design, photophysical properties, and related applications, *iScience*, 2021, **24**, 102858; (*f*) A. Zampetti, A. Minotto and F. Cacialli, Near-infrared (NIR) organic light-emitting diodes (OLEDs): challenges and opportunities, *Adv. Funct. Mater.*, 2019, **29**, 1807623.

2 R. Englman and J. Jortner, The energy gap law for radiationless transitions in large molecules, *Mol. Phys.*, 1970, **18**, 145–164.

3 (*a*) C. You, D. Liu, J. Yu, H. Tan, M. Zhu, B. Zhang, Y. Liu, Y. Wang and W. Zhu, Boosting efficiency of near-infrared emitting iridium(III) phosphors by administrating their π–π conjugation effect of core–shell structure in solution-processed OLEDs, *Adv. Opt. Mater.*, 2020, **8**, 2000154; (*b*) G. Z. Lu, Q. Zhu, L. Liu, Z. G. Wu, Y. X. Zheng, L. Zhou, J. L. Zuo and H. Zhang, Pure red iridium(III) complexes possessing good electron mobility with 1,5-naphthyridin-4-ol derivatives for high-performance OLEDs with an EQE over 31%, *ACS Appl. Mater. Interfaces*, 2019, **11**, 20192–20199; (*c*) C. Y. Kuei, W. L. Tsai, B. Tong, M. Jiao, W. K. Lee, Y. Chi, C. C. Wu, S. H. Liu, G. H. Lee and P. T. Chou, Bis-tridentate Ir(III) complexes with nearly unitary RGB phosphorescence and organic light-emitting diodes with external quantum efficiency exceeding 31%, *Adv. Mater.*, 2016, **28**, 2795–2800; (*d*) Y.-J. Su, H.-L. Huang, C.-L. Li, C.-H. Chien, Y.-T. Tao, P.-T. Chou, S. Datta and R.-S. Liu, Highly efficient red electrophosphorescent devices based on iridium isoquinoline complexes: remarkable external quantum efficiency over a wide range of current, *Adv. Mater.*, 2003, **15**, 884–888; (*e*) Y.-Y. Lyu, J. Kwak, W. S. Jeon, Y. Byun, H. S. Lee, D. Kim, C. Lee and K. Char, Highly efficient red phosphorescent OLEDs based on non-conjugated silicon-cored spirobifluorene derivative doped with Ir-complexes, *Adv. Funct. Mater.*, 2009, **19**, 420–427; (*f*) C.-H. Fan, P. Sun, T.-H. Su and C.-H. Cheng, Host and dopant materials for idealized deep-red organic electrophosphorescence devices, *Adv. Mater.*, 2011, **23**, 2981–2985.

4 K. Li, Y. Chen, J. Wang and C. Yang, Diverse emission properties of transition metal complexes beyond exclusive single phosphorescence and their wide applications, *Coord. Chem. Rev.*, 2021, **433**, 213755.

5 (*a*) F. Wei, S.-L. Lai, S. Zhao, M. Ng, M.-Y. Chan, V. W.-W. Yam and K. M.-C. Wong, Ligand mediated luminescence enhancement in cyclometalated rhodium(III) complexes and their applications in efficient organic light-emitting devices, *J. Am. Chem. Soc.*, 2019, **141**, 12863–12871; (*b*) H. Fukagawa, T. Shimizu, H. Hanashima, Y. Osada, M. Suzuki and H. Fujikake, Highly efficient and stable red phosphorescent organic light-emitting diodes using platinum complexes, *Adv. Mater.*, 2012, **24**, 5099–5103; (*c*) T. Fleetham, G. Li and J. Li, Efficient red-emitting platinum complex with long operational stability, *ACS Appl. Mater. Interfaces*, 2015, **7**, 16240–16246.

6 (*a*) H. Zhang, Z. Chen, L. Zhu, Y. Wu, Y. Xu, S. Chen and W.-Y. Wong, High Performance NIR OLEDs with Emission Peak Beyond 760 nm and Maximum EQE of 6.39%, *Adv. Opt. Mater.*, 2022, **10**, 2200111; (*b*) X. Peng, C.-H. Yeh, S. F. Wang, J. Yan, S. Gan, S.-J. Su, X. Zhou, Y.-X. Zhang and Y. Chi, Near-infrared oleds based on functional pyrazinyl azolate Os(II) phosphors and deuteration, *Adv. Opt. Mater.*, 2022, **10**, 2201291; (*c*) W. Li, B. Wang, T. Miao, J. Liu, X. Lü, G. Fu, L. Shi, Z. Chen, P. Qian and W.-Y. Wong, C1-symmetric [Ir(C^N1)(C^N2)(O^O)]-tris-heteroleptic iridium(III)-complexes with the preferentially horizontal orientation for high-performance near-infrared organic light-emitting diodes, *Adv. Opt. Mater.*, 2021, **9**, 2100117; (*d*) J. Xue, L. Xin, J. Hou, L. Duan, R. Wang, Y. Wei and J. Qiao, Homoleptic facial ir(III) complexes via facile synthesis for high-efficiency and low-roll-off near-infrared organic light-emitting diodes over 750 nm, *Chem. Mater.*, 2017, **29**, 4775–4782; (*e*) Y. Yuan, J.-L. Liao, S.-F. Ni, A. K. Y. Jen, C.-S. Lee and Y. Chi, Boosting efficiency of near-infrared organic light-emitting diodes with Os(II)-based pyrazinyl azolate emitters, *Adv. Funct. Mater.*, 2020, **30**, 1906738; (*f*) Z.-L. Zhu, J.-H. Tan, W.-C. Chen, Y. Yuan, L.-W. Fu, C. Cao, C.-J. You, S.-F. Ni, Y. Chi and C.-S. Lee, High performance NIR OLEDs with low efficiency roll-off by leveraging Os(II) phosphors and exciplex

co-host, *Adv. Funct. Mater.*, 2021, **31**, 2102787; (*g*) Z. Chen, H. Zhang, D. Wen, W. Wu, Q. Zeng, S. Chen and W. Y. Wong, A simple and efficient approach toward deep-red to near-infrared-emitting iridium(III) complexes for organic light-emitting diodes with external quantum efficiencies of over 10, *Chem. Sci.*, 2020, **11**, 2342–2349.

7 (*a*) W.-Y. Hung, C.-J. Yu, L.-W. Fu, C.-L. Ko, B.-K. Su, S.-H. Liu, Y.-C. Kong, P.-T. Chou and Y. Chi, Luminescence of pyrazinyl pyrazolate Pt(II) complexes fine-tuned by the solid-state stacking interaction, *Energy Fuels*, 2021, **35**, 19112–19122; (*b*) P. Ganesan, W. Y. Hung, J. Y. Tso, C. L. Ko, T. H. Wang, P. T. Chen, H. F. Hsu, S. H. Liu, G. H. Lee, P. T. Chou, A. K. Y. Jen and Y. Chi, Functional pyrimidinyl pyrazolate Pt(II) complexes: role of nitrogen atom in tuning the solid-state stacking and photophysics, *Adv. Funct. Mater.*, 2019, **29**, 1900923; (*c*) X. Yang, H. Guo, X. Xu, Y. Sun, G. Zhou, W. Ma and Z. Wu, Enhancing molecular aggregations by intermolecular hydrogen bonds to develop phosphorescent emitters for high-performance near-infrared OLEDs, *Adv. Sci.*, 2019, **6**, 1801930; (*d*) K. H. Kim, J. L. Liao, S. W. Lee, B. Sim, C. K. Moon, G. H. Lee, H. J. Kim, Y. Chi and J. J. Kim, Crystal organic light-emitting diodes with perfectly oriented non-doped Pt-based emitting layer, *Adv. Mater.*, 2016, **28**, 2526–2532; (*e*) K. Tuong Ly, R.-W. Chen-Cheng, H.-W. Lin, Y.-J. Shiau, S.-H. Liu, P.-T. Chou, C.-S. Tsao, Y.-C. Huang and Y. Chi, Near-infrared organic light-emitting diodes with very high external quantum efficiency and radiance, *Nat. Photonics*, 2016, **11**, 63–68; (*f*) Y.-C. Wei, S. F. Wang, Y. Hu, L.-S. Liao, D.-G. Chen, K.-H. Chang, C.-W. Wang, S.-H. Liu, W.-H. Chan, J.-L. Liao, W.-Y. Hung, T.-H. Wang, P.-T. Chen, H.-F. Hsu, Y. Chi and P.-T. Chou, Overcoming the energy gap law in near-infrared OLEDs by exciton–vibration decoupling, *Nat. Photonics*, 2020, **14**, 570–577; (*g*) S.-F. Wang, B.-K. Su, X.-Q. Wang, Y.-C. Wei, K.-H. Kuo, C.-H. Wang, S.-H. Liu, L.-S. Liao, W.-Y. Hung, L.-W. Fu, W.-T. Chuang, M. Qin, X. Lu, C. You, Y. Chi and P.-T. Chou, Polyatomic molecules with emission quantum yields >20% enable efficient organic light-emitting diodes in the NIR(II) window, *Nat. Photonics*, 2022, **16**, 843–850.

8 (*a*) H. B. Gray, S. Záliš and A. Vlček, Electronic structures and photophysics of d^8–d^8 complexes, *Coord. Chem. Rev.*, 2017, **345**, 297–317; (*b*) M. Yoshida and M. Kato, Regulation of metal–metal interactions and chromic phenomena of multi-decker platinum complexes having π-systems, *Coord. Chem. Rev.*, 2018, **355**, 101–115; (*c*) V. M. Miskowski and V. H. Houlding, Electronic spectra and photophysics of platinum(II) complexes with a-diimine ligands. solid-state effects. 2. metal–metal interaction in double salts and linear chains, *Inorg. Chem.*, 1991, **30**, 4446–4452.

9 (*a*) J. A. Bailey, V. M. Miskowski and H. B. Gray, Spectroscopic and structural properties of binuclear platinum-terpyridine complexes, *Inorg. Chem.*, 1993, **32**, 369–370; (*b*) S.-W. Lai, M. C. W. Chan, K.-K. Cheung, S.-M. Peng and C.-M. Che, Synthesis of organoplatinum oligomers by employing N-donor bridges with predesigned geometry: structural and photophysical properties of luminescent cyclometalated platinum(II) macrocycles, *Organometallics*, 1999, **18**, 3991–3997.

10 B. Ma, J. Li, P. I. Djurovich, M. Yousufuddin, R. Bau and M. E. Thompson, Synthetic control of Pt···Pt separation and photophysics of binuclear platinum complexes, *J. Am. Chem. Soc.*, 2005, **127**, 28–29.

11 (*a*) M. Han, Y. Tian, Z. Yuan, L. Zhu and B. Ma, A phosphorescent molecular "butterfly" that undergoes a photoinduced structural change allowing temperature sensing and white emission, *Angew. Chem., Int. Ed.*, 2014, **53**, 10908–10912; (*b*) C. Zhou, Y. Tian, Z. Yuan, M. Han, J. Wang, L. Zhu, M. S. Tameh, C. Huang and B. Ma, Precise design of phosphorescent molecular butterflies with tunable photoinduced structural change and dual emission, *Angew. Chem., Int. Ed.*, 2015, **54**, 9591–9595.

12 (*a*) V. Sicilia, J. Forniés, J. M. Casas, A. Martín, J. A. López, C. Larraz, P. Borja, C. Ovejero, D. Tordera and H. Bolink, Highly luminescent half-lantern cyclometalated platinum(II) complex: synthesis, structure, luminescence studies, and reactivity, *Inorg. Chem.*, 2012, **51**, 3427–3435; (*b*) H. Leopold, M. Tenne, A. Tronnier, S. Metz, I. Münster, G. Wagenblast and T. Strassner, Binuclear C^C* cyclometalated platinum(II) NHC complexes with bridging amidinate ligands, *Angew. Chem., Int. Ed.*, 2016, **55**, 15779–15782; (*c*) S. F. Wang, L.-W. Fu, Y.-C. Wei, S.-H. Liu, J.-A. Lin, G.-H. Lee, P.-T. Chou, J.-Z. Huang, C.-I. Wu, Y. Yuan, C.-S. Lee and Y. Chi, Near-infrared emission induced by shortened Pt–Pt contact: diplatinum(II) complexes with pyridyl pyrimidinato cyclometalates, *Inorg. Chem.*, 2019, **58**, 13892–13901; (*d*) P. Pinter, J. Soellner and T. Strassner, Metallophilic interactions in bimetallic cyclometalated platinum(II) N-heterocyclic carbene complexes, *Eur. J. Inorg. Chem.*, 2021, 3104–3107; (*e*) M. Chaaban, Y. C. Chi, M. Worku, C. Zhou, H. Lin, S. Lee, A. Ben-Akacha, X. Lin, C. Huang and B. Ma, Thiazol-2-thiolate-bridged binuclear platinum(II) complexes with high photoluminescence quantum efficiencies of up to near unity, *Inorg. Chem.*, 2020, **59**, 13109–13116.

13 (*a*) W. Xiong, F. Meng, H. Tan, Y. Wang, P. Wang, Y. Zhang, Q. Tao, S. Su and W. Zhu, Dinuclear platinum complexes containing aryl-isoquinoline and oxadiazole-thiol with an efficiency of over 8.8%: in-depth investigation of the relationship between their molecular structure and near-infrared electroluminescent properties in PLEDs, *J. Mater. Chem. C*, 2016, **4**, 6007–6015; (*b*) X. Wu, Y. Liu, Y. Wang, L. Wang, H. Tan, M. Zhu, W. Zhu and Y. Cao, Highly efficient near-infrared emission from binuclear cyclo-metalated platinum complexes bridged with 5-(4-octyloxyphenyl)-1,3,4-oxadiazole-2-thiol in PLEDs, *Org. Electron.*, 2012, **13**, 932–937; (*c*) N. Su, F. Meng, P. Wang, X. Liu, M. Zhu, W. Zhu, S. Su and J. Yu, Near-infrared emission from binuclear platinum (II) complexes containing pyrenylpyridine and pyridylthiolate units: Synthesis, photo-physical and electroluminescent properties, *Dyes Pigm.*, 2017, **138**, 162–168; (*d*) X. Wu, D. G. Chen, D. Liu, S. H. Liu, S. W. Shen, C. I. Wu, G. Xie, J. Zhou, Z. X. Huang, C. Y. Huang, S. J. Su, W. Zhu and P. T. Chou, Highly Emissive dinuclear platinum(III) complexes, *J. Am. Chem. Soc.*, 2020, **142**,

7469–7479; (*e*) M. Xue, T. L. Lam, G. Cheng, W. Liu, K. H. Low, L. Du, S. Xu, F. F. Hung, D. L. Phillips and C. M. Che, Exceedingly stable luminescent dinuclear Pt(II) complexes with ditopic formamidinate bridging ligands for high-performance red and deep-red oleds with LT_{97}up to 2446 h at 1000 cd m^{-2}, *Adv. Opt. Mater.*, 2022, **10**, 2200741; (*f*) K. W. Lo, G. S. M. Tong, G. Cheng, K. H. Low and C. M. Che, Dinuclear Pt(II) complexes with strong blue phosphorescence for operationally stable organic light-emitting diodes with EQE up to 23% at 1000 cd m^{-2}, *Angew. Chem., Int. Ed.*, 2022, **61**, e202115515; (*g*) B. Ma, P. I. Djurovich, S. Garon, B. Alleyne and M. E. Thompson, Platinum binuclear complexes as phosphorescent dopants for monochromatic and white organic light-emitting diodes, *Adv. Funct. Mater.*, 2006, **16**, 2438–2446; (*h*) W. Xiong, F. Meng, C. You, P. Wang, J. Yu, X. Wu, Y. Pei, W. Zhu, Y. Wang and S. Su, Molecular isomeric engineering of naphthyl-quinoline-containing dinuclear platinum complexes to tune emission from deep red to near infrared, *J. Mater. Chem. C*, 2019, **7**, 630–638.

14 Y. Zhang, J. Miao, J. Xiong, K. Li and C. Yang, Rigid bridge-confined double-decker platinum(II) complexes towards high-performance red and near-infrared electroluminescence, *Angew. Chem., Int. Ed.*, 2022, **61**, e202113718.

15 K. Li, G. S. M. Tong, Q. Wan, G. Cheng, W.-Y. Tong, W.-H. Ang, W.-L. Kwong and C.-M. Che, Highly phosphorescent platinum(II) emitters: photophysics, materials and biological applications, *Chem. Sci.*, 2016, **7**, 1653–1673.

16 X. Feng, J.-G. Yang, J. Miao, C. Zhong, X. Yin, N. Li, C. Wu, Q. Zhang, Y. Chen, K. Li and C. Yang, Au···H–C interactions support a thermally activated delayed fluorescence (TADF) gold(i) complex for OLEDs with little efficiency roll-off and good stability, *Angew. Chem., Int. Ed.*, 2022, **61**, e202209451.

17 A. Chakraborty, J. C. Deaton, A. Haefele and F. N. Castellano, Charge-transfer and ligand-localized photophysics in luminescent cyclometalated pyrazolate-bridged dinuclear platinum(II) complexes, *Organometallics*, 2013, **32**, 3819–3829.

18 (*a*) X. Song, D. Zhang, H. Li, M. Cai, T. Huang and L. Duan, Exciplex system with increased donor–acceptor distance as the sensitizing host for conventional fluorescent OLEDs with high efficiency and extremely low roll-off, *ACS Appl. Mater. Interfaces*, 2019, **11**, 22595–22602; (*b*) Y.-S. Park, S. Lee, K.-H. Kim, S.-Y. Kim, J.-H. Lee and J.-J. Kim, Exciplex-forming co-host for organic light-emitting diodes with ultimate efficiency, *Adv. Funct. Mater.*, 2013, **23**, 4914–4920; (*c*) Y. Seino, H. Sasabe, Y. J. Pu and J. Kido, High-performance blue phosphorescent OLEDs using energy transfer from exciplex, *Adv. Mater.*, 2014, **26**, 1612–1616.

19 (*a*) U. Balijapalli, R. Nagata, N. Yamada, H. Nakanotani, M. Tanaka, A. D'Aleo, V. Placide, M. Mamada, Y. Tsuchiya and C. Adachi, Highly efficient near-infrared electrofluorescence from a thermally activated delayed fluorescence molecule, *Angew. Chem., Int. Ed.*, 2021, **60**, 8477–8482; (*b*) Y. J. Yu, Y. Hu, S. Y. Yang, W. Luo, Y. Yuan, C. C. Peng, J. F. Liu, A. Khan, Z. Q. Jiang and L. S. Liao, Near-infrared electroluminescence beyond 800 nm with high efficiency and radiance from anthracene cored emitters, *Angew. Chem., Int. Ed.*, 2020, **59**, 21578–21584.

